Environmental Pollution 273 (2021) 116428

Contents lists available at ScienceDirect

Environmental Pollution

journal homepage: www.elsevier.com/locate/envpol

Sensitivity of fine particulate matter concentrations in South Korea to regional ammonia emissions in Northeast Asia☆

Eunhye Kim [a], Byeong-Uk Kim [b], Hyun Cheol Kim [c, d], Soontae Kim [a, *]

[a] Department of Environmental & Safety Engineering, Ajou University, Suwon, South Korea
[b] Georgia Environmental Protection Division, Atlanta, GA, 30354, USA
[c] Air Resources Laboratory, National Oceanic and Atmospheric Administration, College Park, MD, 20740, USA
[d] Cooperative Institute for Satellite Earth System Studies, University of Maryland, College Park, MD, 20740, USA

ARTICLE INFO

Article history:
Received 16 November 2020
Accepted 2 January 2021
Available online 5 January 2021

Keywords:
Particulate matter
Long-range transport
Ammonia
Sensitivity
Vertical mixing

ABSTRACT

Ammonia (NH_3) is an important precursor for forming $PM_{2.5}$. In this study, we estimated the impact of upwind transboundary and local downwind NH_3 emissions on $PM_{2.5}$ and its inorganic components via photochemical grid model simulations. Nine sensitivity scenarios with ±50% perturbations of upwind (China) and/or downwind (South Korea) NH_3 emissions were simulated for the year 2016 over Northeast Asia. The annual mean $PM_{2.5}$ concentrations in the downwind area were predicted to change from −3.3 (−18%) to 2.4 $\mu g/m^3$(13%) when the NH_3 emissions in the upwind and downwind areas were perturbed by -50% to +50%. The change in $PM_{2.5}$ concentrations in the downwind area depending on the change in NH_3 emissions in the upwind area was the highest in spring, followed by winter. This was mainly attributed to the change in nitrate (NO_3^-), a secondary inorganic aerosol (SIA) that is a predominant constituent of $PM_{2.5}$. Since NH_3 is mainly emitted near the surface and vertical mixing is limited during the night, it was modeled that the aloft nitric acid (HNO_3)-to-NO_3^- conversion in the morning hours was increased when the NH_3 accumulated near the surface during nighttime begins to mix up within the Planetary Boundary Layer (PBL) as it develops after sunrise. This implies that the control of upwind and/or downwind NH_3 emissions is effective at reducing $PM_{2.5}$ concentrations in the downwind area even under NH_3 rich conditions in Northeast Asia.

1. Introduction

In many countries, emission control policies have been implemented to reduce $PM_{2.5}$ (particulate matter with an aerodynamic diameter smaller than 2.5 μm) due to its adverse effect on public health. In Northeast Asia, known for frequent events of high $PM_{2.5}$ concentration, policies for reducing $PM_{2.5}$ have been focused on the reduction of sulfur dioxide (SO_2) and nitrogen oxides (NOx; precursors of secondary inorganic aerosols (SIAs)) emissions because the fraction of SIAs is large during high $PM_{2.5}$ events (Bae et al., 2019; Huang et al., 2014; Itahashi et al., 2017; Kim et al., 2017a; Zhang et al., 2012). Until recently, tangible achievements as a result of these policies have been reported; for example, Chinese SO_2 emissions decreased by 62% between 2010 and 2017 (Lachatre et al., 2019; Sun et al., 2018; Zheng et al., 2018). However, advanced emission controls, such as flue gas desulfurization (FGD), will likely be required to further reduce SO_2 emissions in the future, and these advanced emission controls can result in significant increases in capital and operating costs for businesses (Zhang et al., 2017).

Some studies have reported that the management of ammonia (NH_3) emissions could be cost-effective for reducing SIA concentrations (Gu et al., 2014; Pinder et al., 2007), although they focused on estimating the impact of NH_3 emission reductions on local $PM_{2.5}$ concentrations (Supplementary Table 1 and references therein). Considering the lifetime and long-range transportation of $PM_{2.5}$ and its precursors (Itahashi et al., 2017; Pinder et al., 2008; Seinfeld and Pandis, 2006), changes in NH_3 emissions in upwind areas could affect concentrations of air pollutants in downwind areas. Once released into the atmosphere, NH_3 can be converted into ammonium (NH_4^+) depending on the atmospheric conditions, e.g. temperature, relative humidity, atmospheric pressure, and availability of other chemicals (Seinfeld and Pandis, 2006). Thus, to estimate the effects of upwind NH_3 changes on downwind air quality, it is

☆ This paper has been recommended for acceptance by Pavlos Kassomenos.
* Corresponding author.
E-mail address: soontaekim@ajou.ac.kr (S. Kim).

https://doi.org/10.1016/j.envpol.2021.116428

Table 1
Upwind and downwind NH_3 emission scenarios.

Case	Upwind (China)	Downwind (South Korea)
C50K50	50%	50%
C50	50%	100%
C50K150	50%	150%
Base	100%	100%
K50	100%	50%
K150	100%	150%
C150K50	150%	50%
C150	150%	100%
C150K150	150%	150%

The simulation period is 1 year (2016).

necessary to understand the fate of atmospheric NHx ($=NH_3 + NH_4^+$) during the long-range transport in lieu of NH_3 (Gilliland et al., 2006). Surface measurements, satellite observations, and air quality model simulation can be used to understand the fate of NHx. A challenge is that current surface observation data for Northeast Asia are available only for very limited spatiotemporal coverage of ambient concentrations and deposition with no vertical distribution information. Space- and airborne measurements can be used to estimate NH_3 vertical distribution, but they exhibit low spatial and temporal resolution over limited spatial and temporal coverage. On the other hand, a three-dimensional photochemical transport model covering a wide range of time and space can be used to explain the emission, transport, and transformation of NHx. Nevertheless, results from modeling often have high uncertainty due to difficulties in acquiring accurate NH_3 emission data (Gilliland et al., 2006; Pinder et al., 2008) in conjunction with insufficient data to verify them. Thus, it is often indispensable to conduct a series of simulations to address uncertainties in the model inputs, such as emissions.

In this study, we attempted to investigate the impact of regional NH_3 emissions on downwind $PM_{2.5}$ concentrations in Northeast Asia using air quality simulations with all available observational data. First, we compared the observed and simulated NH_3, SIA, and $PM_{2.5}$ levels to evaluate the model performance. Second, we examined the sensitivity of the downwind $PM_{2.5}$ concentration to both upwind and downwind NH_3 emissions by using a set of simulations. Third, we analyzed the modeled vertical profiles of NH_3 and NH_4^+ to explain how the upwind NH_3 emission controls can affect downwind areas. Last, we evaluated the effectiveness of future NH_3 emission controls on $PM_{2.5}$ improvements in downwind areas in terms of NH_3 emission uncertainty.

2. Research methods

2.1. Measurement data

We used ground-based observations, including an acid deposition monitoring network (Fig. 1) to examine the concentration of air pollutants in Northeast Asia and verify the simulated concentrations. For China, we used hourly surface $PM_{2.5}$ observations from 1347 sites of the China National Environmental Monitoring Center (CNEMC). For South Korea, we used hourly surface $PM_{2.5}$ and its constituents (including sulfate, nitrate, and ammonium) observations from two supersites, Baengnyeongdo (BR) and Seoul (SD), managed by the National Institute of Environmental Research (NIER). Furthermore, we used gaseous NH_3 observations that were obtained via the filter pack method adopted by the Acid Deposition Monitoring Network in East Asia (EANET) (2016a). Although the original sampling for the EANET data was scheduled daily, we only used the monthly average values due to intermittently available measurements. In addition, our model performance evaluation was limited due to the sparsity of the observation sites (one site located in China, three located in South Korea, and 12 located in Japan). More details about EANET observations can be found in EANET reports (EANET, 2016b).

2.2. Study area and period

Air pollutants can be transported over long distances by westerly winds in Northeast Asia (Itahashi et al., 2017; Li et al., 2007), thus China was set as the upwind area and South Korea as the downwind area. To examine the impact of NH_3 emission changes in the upwind and downwind areas on $PM_{2.5}$ concentrations, the study area covers Northeast Asia (Fig. 1). Specifically, the focus of this study was on the changes in $PM_{2.5}$ and SIA concentrations at the two supersites, BR and SD, in South Korea. The Seoul Metropolitan Area (SMA) represented by SD is a densely populated region with large local emissions. The Chinese contribution to $PM_{2.5}$ concentrations in the SMA has been reported to account for 30–70% (Choi et al., 2019; Kim et al., 2017b), which suggests that the impact of NH_3 emission changes in China and South Korea on $PM_{2.5}$ concentration could be interwoven at SD. On the other hand, BR is located on a small island (~51 km^2) at westernmost South Korea approximately 200 km east of the Shandong Peninsula, China, that has low local emissions of $PM_{2.5}$ and its precursors and is in the pathway of air pollutant transport from China to South Korea throughout the year. For this reason, BR is suitable for examining the transported $PM_{2.5}$ and its precursors from China to South Korea (Jo et al., 2020). The study period was set to the year 2016, and monthly variations of $PM_{2.5}$ and its constituents were analyzed to consider seasonal variability of synoptic meteorology and emissions in Northeast Asia.

2.3. Air quality simulation

For the air quality simulation, a Eulerian photochemical model, Community Multi-scale Air Quality (CMAQ) v4.7.1 was used with a 27-km horizontal resolution over the study area. Furthermore, Process Analysis (PA), which is a probing tool provided by CMAQ, was applied for comprehensive understanding: it enables quantitative evaluation of the physical and chemical processes of air pollutants (Gipson, 1999; Liu et al., 2010). The processes are calculated by applying several terms, such as emissions, advection, diffusion, aerosols, chemistry, clouds, deposition, etc. (Gipson, 1999).

Meteorological input data for CMAQ were prepared by processing the output from the Weather Research and Forecasting (WRF; Skamarock et al., 2008) v3.5.1 simulation using initial/boundary conditions from the Final Operational Global Analysis data (FNL) of the National Centers for Environmental Prediction (NCEP). The number of vertical layers used for our CMAQ model was 22 with the top of the vertical layers located at 50 hPa. The first layer corresponds to approximately 32 m above ground level (AGL). For anthropogenic emissions, the input emission inventories used for this study were the Comprehensive Regional Emissions inventory for Atmospheric Transport Experiment (CREATE) 2015 (Woo et al., 2020) for Northeast Asia excluding South Korea and the Clean Air Policy Support System (CAPSS) 2013 (National Institute of Environmental Research (NIER), 2016) for South Korea; these were processed using the Sparse Matrix Operator Kernel Emission (SMOKE) version 3.1(Benjey et al., 2001). The biogenic emissions were processed using the Model of Emissions of Gases and Aerosols from Nature (MEGAN; Guenther et al., 2006) version 2.04. Further details on the configurations of the simulations can be found in Kim et al., 2021.

One of the study goals was to examine the sensitivity of $PM_{2.5}$

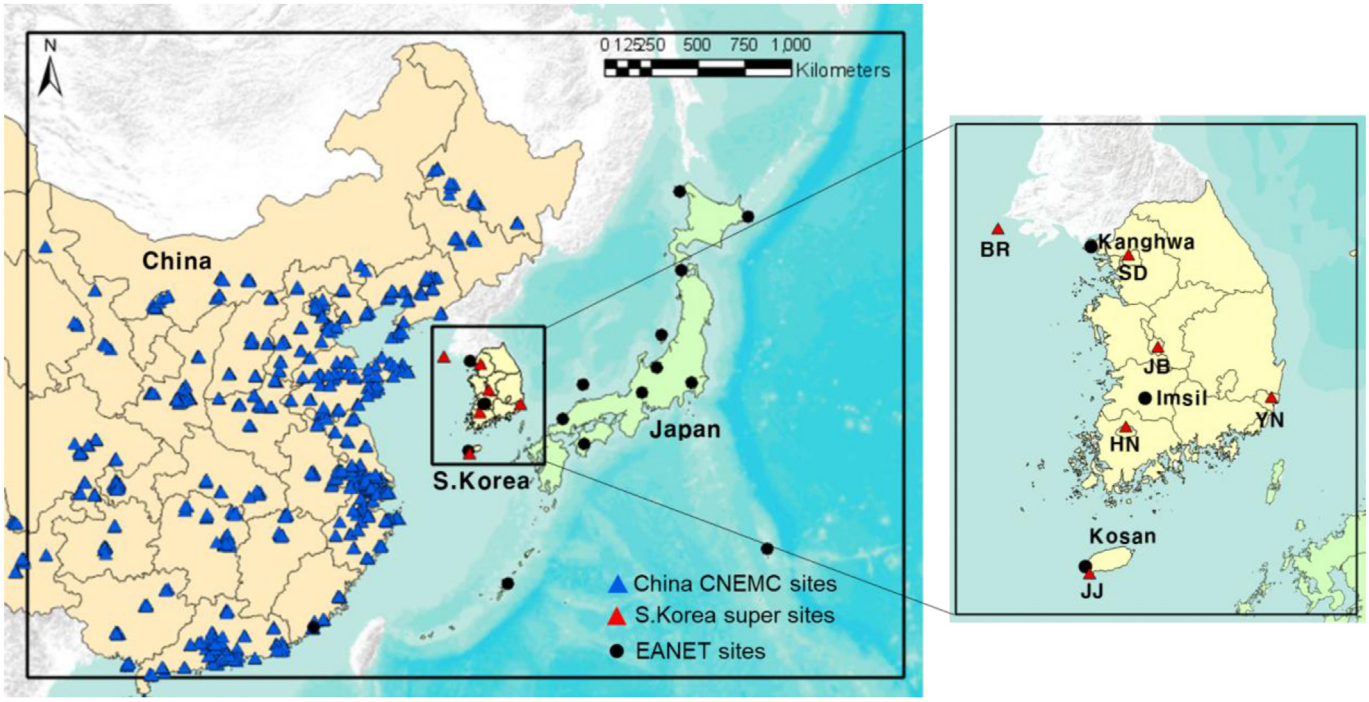

Fig. 1. The modeling domain in this study. The blue and red triangles indicate the locations of the China National Environmental Monitoring Center (CNEMC) sites and South Korean supersites, respectively. Black circles indicate locations of the Acid Deposition Monitoring Network in East Asia (EANET) sites. (For interpretation of the references to color in this figure legend, the reader is referred to the Web version of this article.)

and SIA concentrations in South Korea to NH_3 emission changes in China and South Korea. Therefore, we designed a series of sensitivity tests to understand the dependency of $PM_{2.5}$ concentration on regional (i.e. China and South Korea) and directional (i.e. increasing or decreasing) NH_3 emission changes. We performed a total of 9 simulations, the details of which are reported in Table 1. To clearly identify each sensitivity simulation throughout this manuscript, we applied labels for the sensitivity tests in Table 1 using alphanumeric combinations. The first character of each label represents the region of NH_3 emission changes ("C" for China and "K" for South Korea), while each number following the first character represents the percentage reduction of NH_3 emission compared to the base simulation. For example, C50 denotes a 50% reduction in NH_3 emission in China while K150 means a 50% increase in NH_3 emission in South Korea compared to the base simulation. We used two alphanumeric labels back-to-back to signify that the NH_3 emissions in the two regions were changed simultaneously. For example, C50K150 means a 50% reduction in Chinese NH_3 emission as well as a 50% increase in South Korean NH_3 emission. The base simulation was used to examine the monthly variations in $PM_{2.5}$ and SIA concentration sensitivities to regional NH_3 emissions in 2016.

To evaluate how uncertainties in NH_3 emissions significantly affect $PM_{2.5}$ changes, an additional 16 cases with ±25% perturbations of the NH_3 emissions in China and South Korea (Supplementary Table 2) were modeled for January, April, July, and October.

3. Results

3.1. Model performance evaluation

3.1.1. Surface $PM_{2.5}$ and SIA

In 2016, the annual average observed $PM_{2.5}$ concentrations in China and South Korea were 49 and 26 $\mu g/m^3$ (Supplementary Table 3) while the simulated concentrations were 51 and 25 $\mu g/m^3$, respectively. That is to say, the modeled concentrations were overestimated by 4% in China and underestimated by 4% in South Korea. In both China and South Korea, the observed concentrations during the cold seasons (spring and winter) were higher than those during the warm season (summer). The simulated $PM_{2.5}$ concentrations closely followed the observed seasonal variabilities of $PM_{2.5}$ concentrations on average across all monitoring stations (Supplementary Fig. 1). The same seasonal variabilities of $PM_{2.5}$ concentrations were observed at BR (12.4–31.3 $\mu g/m^3$) and SD (15.9–35.3 $\mu g/m^3$) (Supplementary Fig. 2 and Supplementary Table 4). Nitrate (NO_3^-; 0.2–3.6 $\mu g/m^3$ at BR and 1.0–8.2 $\mu g/m^3$ at SD) is one of the key components driving $PM_{2.5}$ changes in the region, suggesting that the seasonal variability of $PM_{2.5}$ concentration depends on NO_3^- variability which, in turn, depends on the temperature and humidity (Morino et al., 2006). On the other hand, sulfate (SO_4^{2-}; BR: 1.8–8.4 $\mu g/m^3$ and SD: 3.2–7.4 $\mu g/m^3$) showed the opposite seasonal variability (the concentration being higher in summer and lower in spring and winter) (Bae et al., 2019), which suggests that its variation is due to the oxidation of SO_2 to SO_4^{2-} in summer (Seinfeld and Pandis, 2006). The SO_4^{2-} concentrations at BR and SD were similar while the NO_3^- concentration was higher at SD than at BR, which likely indicates that NO_3^- in the downwind area is affected not only by the upwind emissions but also the downwind emissions (Kim et al., 2021).

3.1.2. Surface NH_3

The NH_3 concentrations observed by EANET and predicted by the simulation over Northeast Asia were compared before examining the sensitivity of $PM_{2.5}$ and SIA concentrations under various upwind and downwind NH_3 emission conditions (Supplementary Fig. 3). The observations during the study period show that NH_3

concentration was the highest in China (10.7 ppb), followed by South Korea (3.0 ppb), and Japan (1.0 ppb). Similarly, the simulated NH_3 concentration was the highest in China, followed by South Korea, and Japan. On average across all monitors, the simulated NH_3 concentration was overestimated by 0.2 ppb compared to the observed concentration in South Korea and was underestimated by 6.1 and 0.5 ppb in China and Japan, respectively. It should be noted that there is only one EANET observation station in China (Fig. 1), thus the observed NH_3 concentrations may not be representative over all of China.

In South Korea, the highest NH_3 concentration was observed at Imsil, which is located inland, while the lowest NH_3 concentration was observed at Kanghwa, which is located approximately 150 km away from BR and where NH_3 observations are not available (Fig. 1 and Supplementary Fig. 4). Both the observed and simulated concentrations of NH_3 at Kanghwa were around 0.8 ppb. Since the simulated NH_3 concentration at BR was lower than that at Kanghwa, which is located closer to the inland area of South Korea, it was assumed that the NH_3 concentration at BR was as low as that at Kanghwa (Supplementary Fig. 5).

The spatiotemporal distributions of the simulated NH_3, SIA, and $PM_{2.5}$ concentrations showed good agreement with those of the observed concentrations (as discussed in Section 3.1), so the simulations in this study can be used confidently to explain $PM_{2.5}$ sensitivity to NH_3 emissions, as discussed in the next section.

3.2. $PM_{2.5}$ sensitivity to NH_3 emissions

3.2.1. Annual mean $PM_{2.5}$

NH_3 sensitivity simulations show that the changes in the annual average $PM_{2.5}$ concentrations according to the NH_3 emission changes in China and/or South Korea ranged from −3.9 (−16%; C50K50) to 2.2 $\mu g/m^3$ (9%; C150K150) in China and from −3.3(−18%; C50K50) to 2.4 $\mu g/m^3$(13%; C150K150) in South Korea when compared to the base simulation (Supplementary Fig. 6). In South Korea, the $PM_{2.5}$ concentration decreased as NH_3 emissions decreased (−9% in both C50 and K50). A similar decrease in $PM_{2.5}$ concentration in South Korea according to NH_3 emission reduction in both China and South Korea suggests that the NH_3 emission changes not only in the downwind area but also in the upwind areas are important for determining the $PM_{2.5}$ concentration in the downwind area.

When the directions of the NH_3 emission changes are opposite for China and South Korea (such as in C50K150 and C150K50), the $PM_{2.5}$ sensitivity of South Korea to NH_3 emissions varied depending on the region (Fig. 2 and Supplementary Fig. 7). In general, the NH_3 emission change in South Korea had a dominant impact on the annual average $PM_{2.5}$ concentration in South Korea, including SD. Meanwhile, the NH_3 emission change in China had a dominant impact on the $PM_{2.5}$ concentration changes in the South Korean regions close to China, such as BR.

3.2.2. Monthly concentration variation of $PM_{2.5}$ and its components

$PM_{2.5}$ concentration has seasonal variability in South Korea and its main components, sulfate, nitrate, and ammonium, vary depending on the season (Bae et al., 2019; Choi et al., 2012; Lee et al., 1999). Hence, we examined the monthly concentration variations of $PM_{2.5}$ and its components according to NH_3 emission changes.

As shown in Fig. 3, the change in $PM_{2.5}$ concentrations was high during the cold season, ranging from −29% to 17% at BR. This is because, during the cold season, (1) NH_3 emissions were high in China, especially in March and April (Supplementary Table 5) (Zheng et al., 2018b); (2) meteorological conditions such as temperature and relative humidity were suitable for secondary aerosol formation (Seinfeld and Pandis, 2006); and (3) long-range transport from China to South Korea became more frequent via the continental outflow during the season (Lin et al., 2010). Meanwhile, changes in $PM_{2.5}$ concentration were relatively low in July and August, which can be attributed to the frequent precipitation that occurred during these months (Supplementary Fig. 8) because more precipitation increased the wash-out and resulted in a weak influence by the long-range transportation (Li et al., 2007). Furthermore, under the high-temperature conditions in July and August, NO_3^- (the main component of $PM_{2.5}$) was easily converted back into nitric acid (HNO_3) (Seinfeld and Pandis, 2006). The change in $PM_{2.5}$ concentration at SD was also large in the cold season (−17%–12%), which is similar to the results at BR.

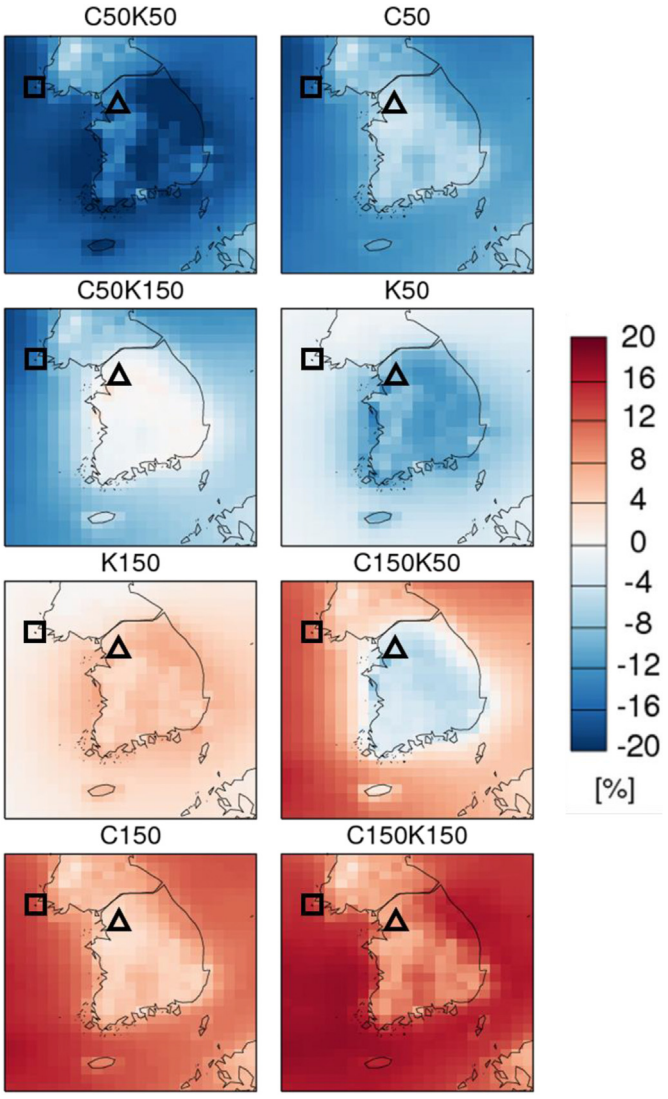

Fig. 2. Spatial plots of relative annual $PM_{2.5}$ changes between the base and sensitivity simulation cases for Korea. The square is the location of the Baengnyeongdo (BR) supersite, and the triangle is that of the Seoul (SD) supersite. BR and SD showed opposite signs for $PM_{2.5}$ sensitivity to NH_3 in C150K150.

3.2.3. Daily mean $PM_{2.5}$ concentration sensitivity

Considering that the purpose of $PM_{2.5}$ management is to protect against its adverse health effects, the reduction of short-term $PM_{2.5}$ concentration, as well as long-term $PM_{2.5}$ concentration, is

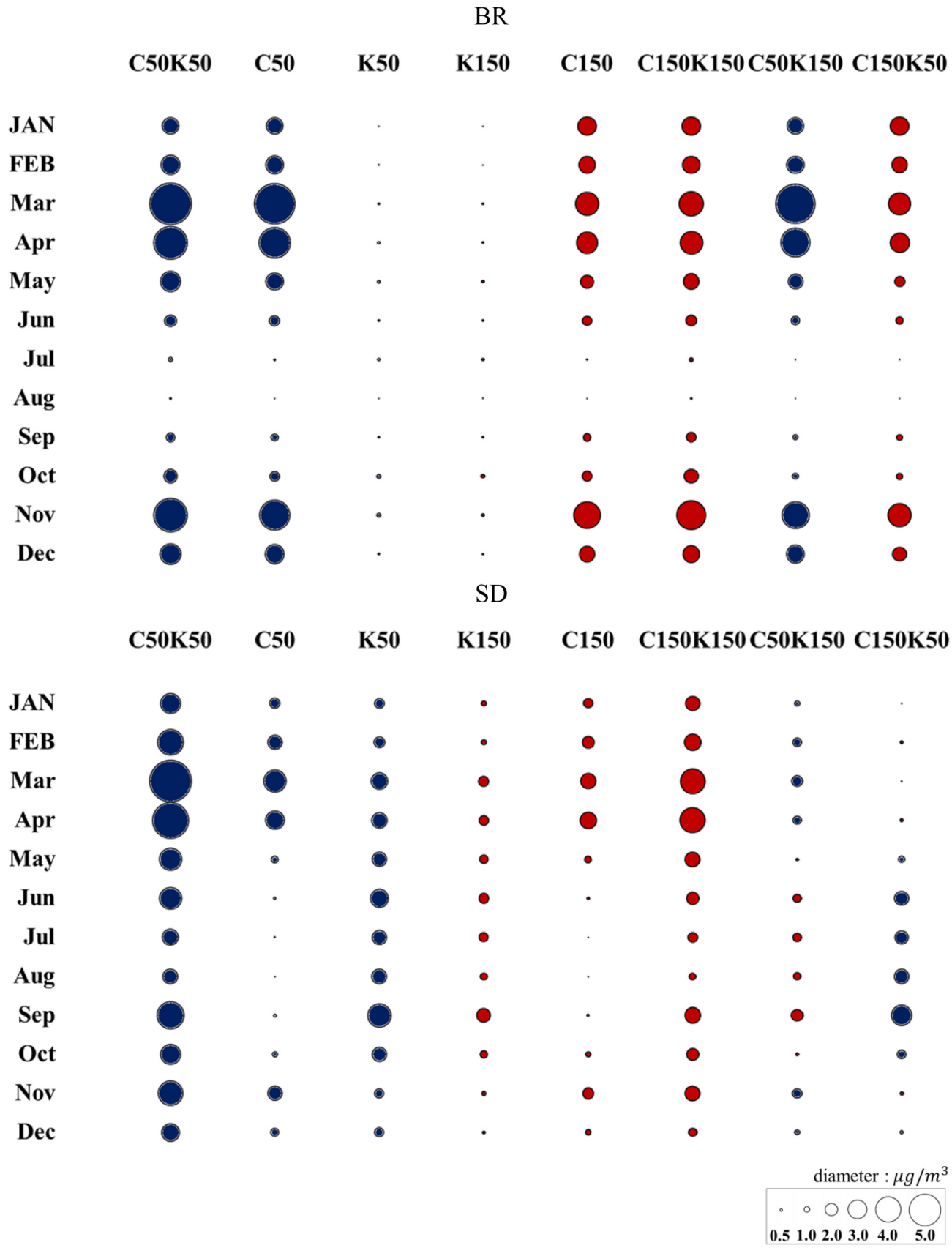

Fig. 3. Bubble charts of $PM_{2.5}$ sensitivity to ammonia (NH_3) emission perturbations at the Baengnyeongdo (BR; top) and Seoul (SD; bottom) supersites under various scenarios (Table 1). The diameter for each circle signifies the magnitude of $PM_{2.5}$ sensitivity. Red means an increase in $PM_{2.5}$ concentration while blue means a decrease because of NH_3 emission changes. (For interpretation of the references to color in this figure legend, the reader is referred to the Web version of this article.)

important because the former can cause acute health effects.

In this study, the sensitivity of daily $PM_{2.5}$ concentrations to NH_3 emission changes was evaluated in the short-term. Fig. 4 shows changes in the simulated daily mean $PM_{2.5}$ concentrations at BR and SD according to NH_3 emission changes in China and South Korea. When the simulated daily mean $PM_{2.5}$ concentration (x-axis) was higher, the change in $PM_{2.5}$ concentration (y-axis) according to NH_3 emission change was higher. When a concentration of 50 $\mu g/m^3$ or higher occurred, the change in $PM_{2.5}$ concentration ranged from −17.83(−27%; C50K50) to 11.34 $\mu g/m^3$(17%; C150K150) at BR and from −15.12(−24%; C50K50) to 9.02 $\mu g/m^3$(14%; C150K150) at SD. These results imply that reducing NH_3 emissions can effectively reduce the $PM_{2.5}$ concentration, especially when a high $PM_{2.5}$ concentration occurs in South Korea where the daily $PM_{2.5}$ standard is frequently exceeded.

The absolute values of the slope of the regression lines are presented to compare the magnitude of $PM_{2.5}$ sensitivity to NH_3 emission change in terms of $PM_{2.5}$ level. At BR, the values are high in the order of NH_3 emission reduction in China (C50; 0.29), NH_3 emission increase in China (C150; 0.20), and NH_3 emission reduction in South Korea (K50; 0.09). This result indicates that the $PM_{2.5}$ concentration at BR is generally more sensitive to NH_3 emission change in China than in South Korea.

3.3. Inorganic aerosols and ammonia

3.3.1. Sulfate and nitrate

Since $PM_{2.5}$ changes are mainly driven by changes in NO_3^- and NH_4^+ concentrations (Supplementary Fig. 9), the sensitivity of SIAs to NH_3 emissions was evaluated. In Fig. 5, the maximum simulated changes of monthly SO_4^{2-} concentrations according to changes in NH_3 emissions in March were 0.71 and 0.69 $\mu g/m^3$ at BR and SD, respectively. However, these changes are small compared to the changes in NO_3^- concentration because NH_3 emission changes have a bigger impact on the conversion of HNO_3 to NO_3^- than sulfuric acid (H_2SO_4) to SO_4^{2-}2- (Pinder et al., 2008). HNO_3 and H_2SO_4, which are the oxidized forms of NOx and SO_2, respectively, are neutralized by NH_3 and then converted to ammonium nitrate (NH_4NO_3) and ammonium sulfate ($(NH_4)_2SO_4$), respectively (Seinfeld and Pandis, 2006). SO_2 is oxidized by either gaseous-phase oxidation or aqueous-phase oxidation involving oxidants such as hydrogen peroxide (H_2O_2) and ozone (O_3). Gaseous-phase oxidation is rarely affected by NH_3 concentration, and although the latter changes the pH, which can affect the aqueous-phase equilibrium concentrations (especially for the reaction with O_3), the solubility of H_2O_2, which is abundant in clouds and fog, is hardly affected by pH changes (Seinfeld and Pandis, 2006). Therefore, the SO_4^{2-} concentration is not very sensitive to NH_3 or NH_4^+ concentration changes (Itahashi et al., 2019; Wang et al., 2013). That is why the change of SO_4^{2-} concentration was not significant in this study even if the NH_3 concentration falls to half that of the base simulation in China and South Korea.

Meanwhile, HNO_3 in the gaseous phase is transferred to the aqueous phase and then converted to NO_3^-. This as an aerosol can be partly partitioned to gaseous HNO_3 depending on the environmental conditions, including the pH of the liquid phase. As shown in Fig. 5, the maximum changes in monthly NO_3^- concentrations according to NH_3 emission changes at SD in September were 4.72 .(58% of the NO_3^- concentration) at BR in March and 2.51 $\mu g/m^3$(27% of the NO_3^- concentration). In addition to NO_3^- transported from China, NO_3^- at SD is formed from the reaction between the intermediate species (i.e. HNO_3), which are domestically emitted or transported from the upwind area, and NH_3 occurring in South Korea (Chen et al., 2014; Kim et al., 2021), which is one of the reasons why the NO_3^- changes at SD is smaller than those at BR according to NH_3 emission changes. This is discussed in detail in Section 3.3.2.

3.3.2. NH_3 and NH_4^+

The NH_3 concentrations and the NH_4^+/NHx ratio were examined to understand the form of NHx (NH_3 and NH_4^+) during long-range transport (which is important for forming NO_3^-). As shown in Fig. 5, the simulated surface NH_3 concentration at SD showed monthly variability ranging from 5.9 to 10.6 ppb, while the NH_3 concentration at BR was lower than 1 ppb due to low emissions from the surrounding area. Thus, the conversion of HNO_3 to NH_4NO_3 at BR was limited by the low NH_3 concentration.

NH_3 concentration changes at SD were from −0.9 (C50) to

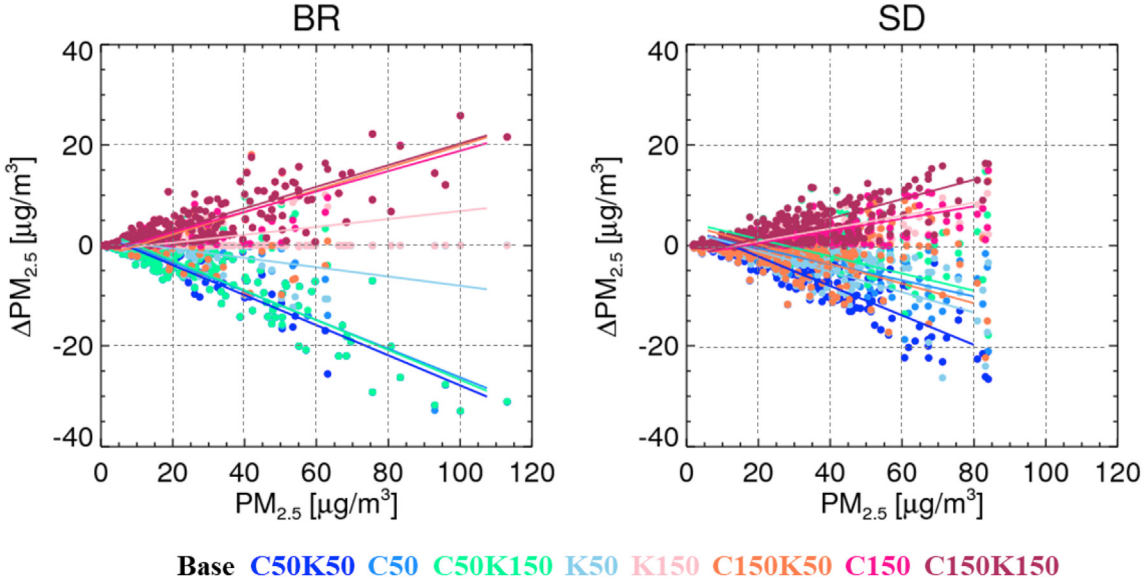

Fig. 4. Scatter plots of paired $PM_{2.5}$ concentrations and $PM_{2.5}$ concentration changes at the Baengnyeongdo (BR; left) and Seoul (SD; right) supersites in 2016 for various scenarios of NH_3 emission perturbation (Table 1).

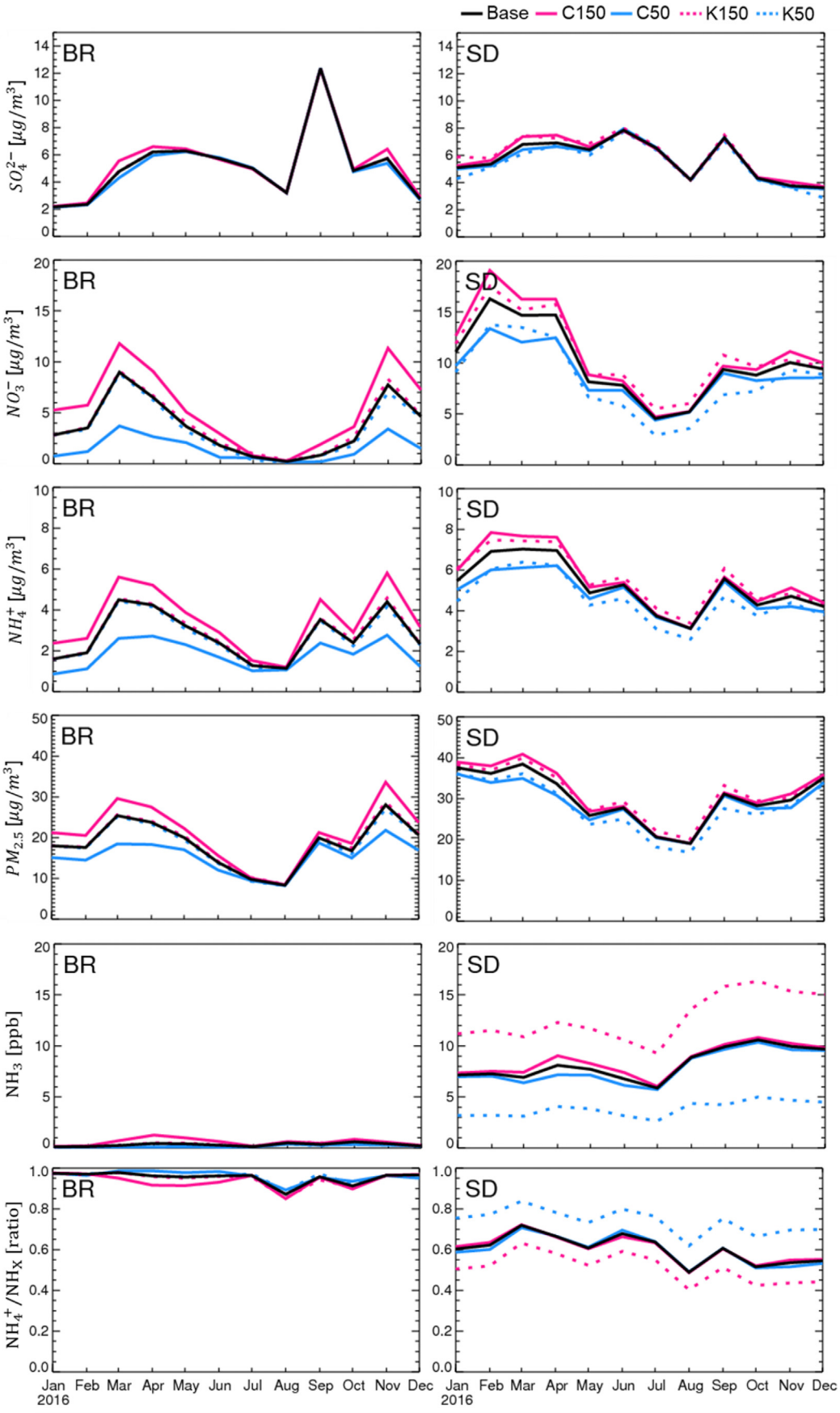

Fig. 5. Monthly variations in sulfate (SO_4^{2-}), nitrate (NO_3^-), ammonium (NH_4^+), $PM_{2.5}$, and ammonia (NH_3) concentrations and the NH_4^+/NHx ratio at the Baengnyeongdo (BR; left) and Seoul (SD; right) supersites. Base; C150, a 50% Chinese NH_3 emission increase; C50, a 50% Chinese NH_3 emission decrease, K150, a 50% Korean NH_3 emission increase; K50, a 50% Korean NH_3 emission decrease.

0.9 ppb (C150) and from −5.7 (K50) to 5.9 ppb (K150) when the NH_3 emissions were changed in China and South Korea, respectively. At BR, the simulated ratio of NH_4^+ to NHx can reach 0.9 or more in most seasons, which suggests that NHx transported from China to South Korea is mostly NH_4^+.

On the contrary, the ratio of NH_4^+ to NHx at SD was much lower than at BR, which suggests that free NH_3 exists without being converted to NH_4^+ since a large amount of NH_3 is emitted in and around the SD. The NH_3 conditions (rich or poor) was estimated via the Adjusted Gas Ratio (AdjGR) at BR and SD (Supplementary Figs. 10 and 11), which is the molar ratio of free ammonia to total nitrate concentration (Pinder et al., 2008) as follows:

$$AdjGR = \frac{[Free\ ammonia]}{[total\ nitrate]} = \frac{[NH_3] + [NO_3^-]}{[NO_3^-] + [HNO_3]} \quad (1)$$

An AdjGR value of less than 1 is an indication of NH_3-poor conditions, while an AdjGR value of greater than 1 indicates the opposite. Most simulations in this study (except for C50K150, C150, and C150K150 for March, April, and May) showed NH_3-poor conditions at BR, which suggests that most of the NH_3 had already been converted to NH_4^+ upwind. This is consistent with the results presented in Fig. 5. Since the available NH_3 was limited at BR, it is difficult for the intermediate species transported from China (such as HNO_3) to form NO_3^- at and around BR. On the other hand, transported HNO_3 is likely to be converted into NO_3^- in and around SD because the areas near SD are NH_3-rich (Kim et al., 2021).

3.4. Long-range transport and vertical mixing

Surface NO_3^- concentration is affected by aloft chemical reactants due to vertical mixing (Kim et al., 2021; Lee et al., 2019). Thus, it is important to understand vertical distributions of the chemical reactants when estimating the sensitivity of surface NO_3^- to NH_3 emission, and so we estimated the dynamics of the vertical distributions of NH_3, HNO_3, and NO_3^- that depend on the change in Planetary Boundary Layer (PBL) between daytime and nighttime (Zhao et al., 2016).

During the night when vertical mixing is limited, the transported HNO_3 above the PBL at 1–2 km increased (Supplementary Fig. 12 (middle)) whereas the transported NO_3^- decreased (Supplementary Fig. 13 (middle)) when NH_3 emission from China was decreased (the C50 scenario). However, during the daytime when the PBL becomes higher, the decrease in NO_3^- impacts on the surface via vertical mixing because air pollutants are vertically well mixed within the PBL (Supplementary Fig. 13 (middle)). Thus, a decrease in NH_3 emission from China caused a decrease in surface NO_3^- concentration at SD.

When NH_3 emissions in South Korea were decreased (K50), the HNO_3 and NO_3^- concentration changes at the surface were small during the nighttime (Supplementary Figs. 12 (bottom) and 13 (bottom)). This is because the NH_3 at SD was still abundant near the surface despite a 50% reduction in NH_3 emissions in South Korea (Supplementary Figs. 11 and 14 (bottom). Meanwhile, the surface NO_3^- decreased during the daytime (Supplementary Fig. 13 (bottom)). Although NH_3 was abundant at the surface, this was not the case in the upper layer (Supplementary Fig. 15). Therefore, the decrease in NH_3 emission limited the formation of NO_3^- in the upper layer, which then caused the decrease in surface NO_3^- concentration by vertical mixing during the daytime.

To support this reasoning, the physical processes of forming the base NH_3, HNO_3, and NO_3^- concentrations by using PA for April as a representative month of spring when the NO_3^- concentration was high and the long-range transport was frequent (Bae et al., 2019). In Fig. 6, the NO_3^- concentration aloft has a positive sign whereas the HNO_3 concentration aloft has a negative sign during the daytime by particle formation process, which means that much of the HNO_3 was converted to NO_3^-. This is possible because the NH_3 was mixed up as a result of the PBL increase, which converted HNO_3 aloft to NO_3^-. Since surface NH_3, which can convert HNO_3 to NO_3^-, is abundant at SD, we suppose that the HNO3 aloft was transported in the upper air. Meanwhile, the increase in HNO_3 concentration near the surface during the daytime was because of the partitioning of NO_3^- and HNO_3 (Fig. 6), which can be attributed to an increase in temperature during the daytime. However, aircraft-based observations for NH_3, HNO_3, and NO_3^- are required in the future to verify these assumptions.

Fig. 7 shows a summary of the fate of NH_3, HNO_3, and NO_3^- during the daytime and nighttime regardless of NH_3 emission change. NH_3 concentrations were high below the PBL, particularly near the surface at night (the left panel in Fig. 7 and Supplementary Fig. 14 (top)) because the PBL was low during the night and the vertical mixing was limited. Thus, NH_3 mainly accumulated at the surface during the night. In contrast to NH_3, the HNO_3 concentration was low at the surface during the night (the left panel in Fig. 7 and Supplementary Fig. 12 (top)) because HNO_3 was converted to NO_3^- by NH_3, the concentration of which was high at the surface. As the PBL grew during the daytime (right panel in Fig. 7), NH_3 at the surface was mixed up, thereby enabling it to convert aloft HNO_3 to NO_3^-. The converted NO_3^- aloft can be mixed down by vertical mixing, which then increased the NO_3^- concentration at the surface.

3.5. Sensitivity to NH_3 emission uncertainty

We estimated the changes in $PM_{2.5}$ concentration at SD according to NH_3 emission changes in China and South Korea by considering the NH_3 emission uncertainties. Fig. 8 shows the impact of NH_3 emission reduction on $PM_{2.5}$ concentration in April 2016. We assumed that $PM_{2.5}$ concentrations in the real world ranged from "a" to "i" in Fig. 8 by simulations with 25% NH_3 emission uncertainties in China and South Korea.

The $PM_{2.5}$ concentration denoted as "e" in Fig. 8 is the simulated concentration with no NH_3 emission change from the emissions inventory; it decreased by 1.5 $\mu g/m^3$ under a 25% NH_3 emission reduction in China (e to h) and by 1.0 $\mu g/m^3$ under a 25% NH_3 emission reduction in South Korea (e to d). The $PM_{2.5}$ concentration at SD decreased by 1.6 $\mu g/m^3$ during the 25% NH_3 emission reduction in China (c to c') and by 0.9 $\mu g/m^3$ during the 25% NH_3 emission reduction in South Korea (c to c") under "c", assuming that the real NH_3 emissions were 25% higher than the base simulation in both China and South Korea (the NH_3 emission reduction rate corresponding to 20% from "c" was converted to 25%). Under "g", the $PM_{2.5}$ concentrations at SD decreased by 1.1 (g to g') and 1.1 $\mu g/m^3$ (g to g"), respectively, assuming that the real NH_3 emissions were 25% lower than the base simulation in both China and South Korea (the NH_3 emission reduction rate corresponding to 33% from "g" was converted to 25%). These can be mainly attributed to the nitrate level in $PM_{2.5}$ (Supplementary Fig. 16).

We found that the NH_3 emission reductions both upwind and downwind effectively reduced the $PM_{2.5}$ concentrations in the downwind area (Supplementary Table 6) and the effects of decreased $PM_{2.5}$ or NO_3- were similar among the cases even though there were NH_3 emission uncertainties both upwind and downwind. Moreover, as shown in Supplementary Fig. 17, NH_3 emission reduction in China was more effective in January and April when $PM_{2.5}$ concentrations over the downwind area were higher than those in other months because the concentration of NH_3 decreased as the SIA concentration increased (Lachatre et al., 2019) when there was a high $PM_{2.5}$ concentration at SD.

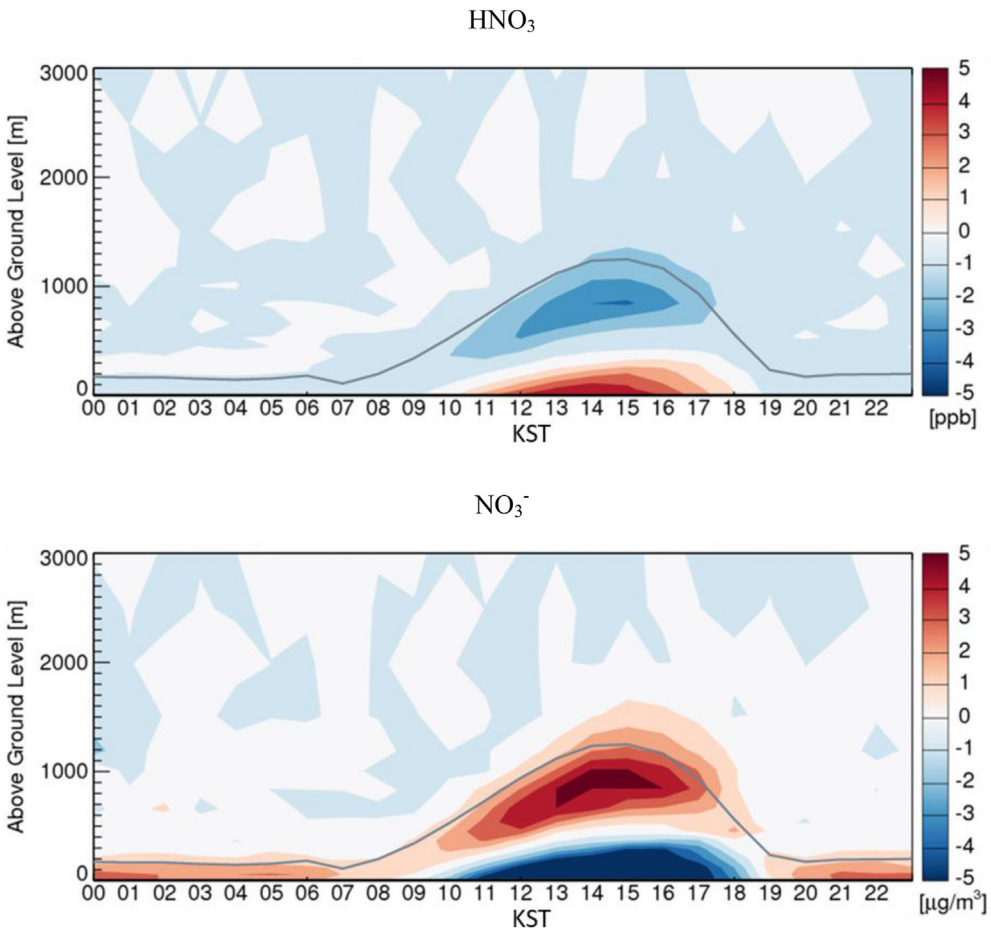

Fig. 6. Vertical distributions of the formation of nitric acid (HNO_3; top) and nitrate (NO_3^-; bottom) at the Seoul (SD) supersite in April 2016. The gray line represents the Planetary Boundary Layer (PBL) height.

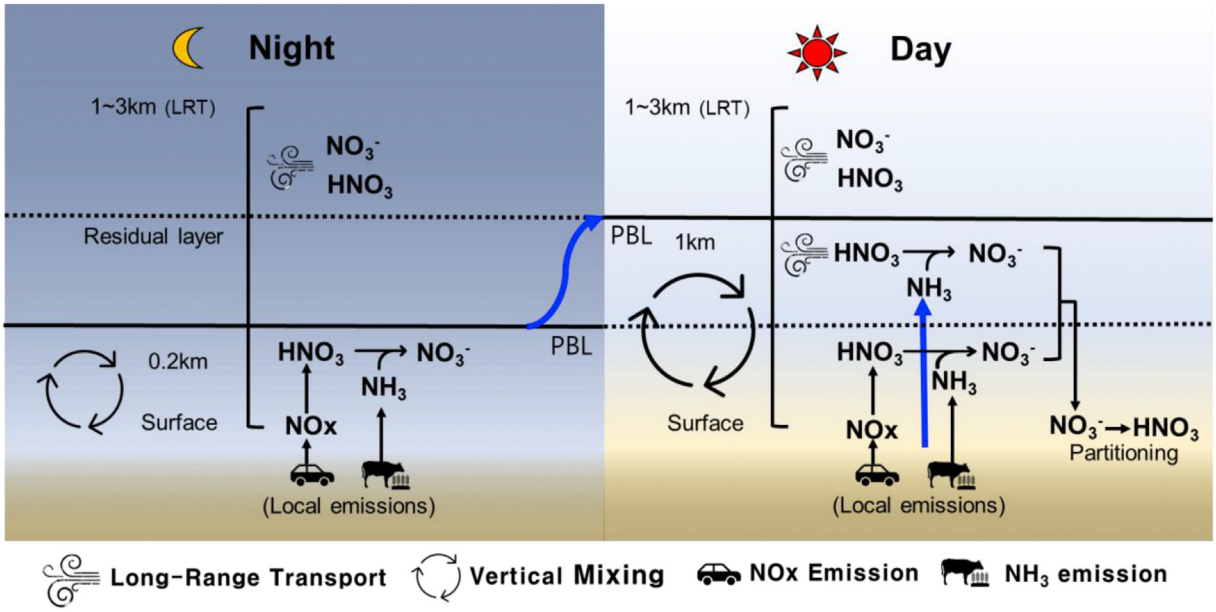

Fig. 7. A schematic of the fate of ammonia (NH_3), nitrogen oxides (NOx), nitric acid (HNO_3), and nitrate (NO_3^-) during nighttime (left) and daytime (right) in the downwind area.

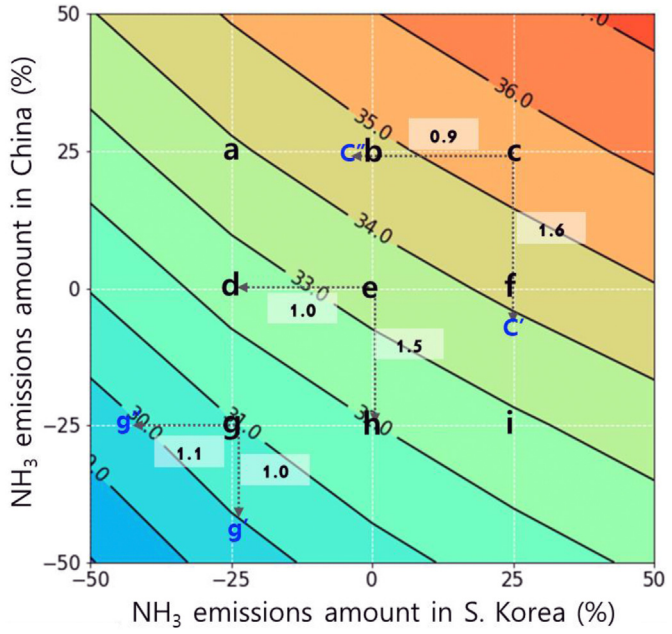

Fig. 8. $PM_{2.5}$ isopleths for China and South Korea's ammonia (NH_3) emission changes at Seoul (SD) in April 2016. Each alphabet character represents the uncertainty of NH_3 emissions: (') means a 25% reduction in the Chinese NH_3 emission and (") means a 25% reduction in the South Korean NH_3 emission.

4. Conclusions

We investigated regional-scale spatiotemporal variations of downwind $PM_{2.5}$ sensitivity to changes in upwind (China) and downwind (South Korea) NH_3 emissions in Northeast Asia using a series of simulations for the year 2016. The annual average $PM_{2.5}$ concentration changes in South Korea varied from −1.6 (−9%) to 1.4 $\mu g/m^3$ (8%) when the relative NH_3 emission changes in China were varied from −50% to +50%. For relative NH_3 emission changes ranging from −50% to +50% in South Korea, the annual average $PM_{2.5}$ concentration changes in South Korea ranged from −1.7 (−9%) to 1.1 $\mu g/m^3$ (6%). The impact of NH_3 emission changes in the upwind area on $PM_{2.5}$ concentrations in the downwind area showed seasonal variations: the highest in spring followed by winter. These changes were mainly attributed to NO_3^-, which is one of the $PM_{2.5}$ constituents.

The vertical structure of NO_3^- concentration over the downwind area was examined to understand the fate and formation of NO_3^- in downwind areas in relation to $PM_{2.5}$ precursor (e.g. NOx and NH_3) emissions and their intermediate reaction products (e.g. HNO_3) in Northeast Asia. Our simulation results show that NH_3 emitted from surface-level sources (i.e. agriculture and automobiles) in the downwind area accumulated during nighttime when deep vertical mixing was limited. When the PBL started to grow in the morning, accumulated NH_3 near the ground could mix well within PBL. Most NOx is converted to HNO_3, which is emitted in downwind areas and converted to NH_4NO_3 because NH_3 is abundant at the surface. Meanwhile, the HNO_3 transported from the upwind area through the free atmosphere often stays in the residual layer during nighttime over the downwind area. Eventually, the vertically well-mixed NH_3 reacts with the locally available and transported HNO_3 and forms NH_4NO_3. In addition, at the downwind area, the NO_3^- formed in the upwind area or during transportation is mixed with local air parcels when the PBL grows in the downwind area, which results in an increase in the surface NO_3^- concentration.

Meanwhile, the $PM_{2.5}$ sensitivity to NH_3 emissions was similar among the simulations when assuming an NH_3 emission uncertainty. Thus, decreasing the $PM_{2.5}$ concentration by controlling the NH_3 emissions can be assumed even though there are uncertainties in the NH_3 emissions both upwind and downwind.

Traditionally, emission control policies to reduce secondary air pollutants, including $PM_{2.5}$, have focused on managing species that are apparently reaction-limiting, i.e. a less abundant precursor based on emissions. However, our study results show that controlling the emission of NH_3, the most abundant $PM_{2.5}$ precursor emitted in Northeast Asia, can be effective for decreasing the $PM_{2.5}$ concentration in South Korea, the downwind area in the region. We suggest that a paradigm shift in emission control policies should be sought by examining the dynamics of the vertical distributions of precursors and intermediates between the upwind and downwind areas in the future.

Author statement

Eunhye Kim: Conceptualization, Investigation, Visualization, Writing- Original draft. Byeong-Uk Kim: Conceptualization, Writing- Reviewing & Editing. Hyun Cheol Kim: Software, Writing-Reviewing & Editing. Soontae Kim: Writing- Original draft, Supervision.

Discalimer

The scientific results and conclusions, as well as any views or opinions expressed herein, are those of the author(s) and do not necessarily reflect the views of NOAA or the Department of Commerce.

Declaration of competing interest

The authors declare that they have no known competing financial interests or personal relationships that could have appeared to influence the work reported in this paper.

Acknowledgments

This work was supported by the National Air Emission Inventory and Research Center (NAIR); and Korea Ministry of Environment (MOE) as Graduate School specialized in Climate Change.

Appendix A. Supplementary data

Supplementary data to this article can be found online at https://doi.org/10.1016/j.envpol.2021.116428.

References

Bae, C., et al., 2019. Long-range transport influence on key chemical components of PM2.5 in the Seoul metropolitan area, South Korea, during the years 2012–2016. Atmosphere 11, 48.
Benjey, W., et al., 2001. Implementation of the SMOKE Emission Data Processor and SMOKE Tool Input Data Processor in Models-3. US EPA.
Chen, T.-F., et al., 2014. Modeling direct and indirect effect of long range transport on atmospheric PM2.5 levels. Atmos. Environ. 89, 1–9.
Choi, J., et al., 2019. Impacts of local vs. trans-boundary emissions from different sectors on PM2.5 exposure in South Korea during the KORUS-AQ campaign. Atmos. Environ. 203, 196–205.
Choi, J.-K., et al., 2012. Chemical characteristics of PM2.5 aerosol in incheon, Korea. Atmos. Environ. 60, 583–592.
EANET, 2016a. Acid Deposition Monitoring Network in East Asia. https://monitoring.eanet.asia/document/public/index;. (Accessed 6 October 2020).
EANET: Data Report 2016, available at: 2016, last access: 6 October 2020.
Gilliland, A.B., et al., 2006. Seasonal NH3 emissions for the continental United States: inverse model estimation and evaluation. Atmos. Environ. 40, 4986–4998.
Gipson, G.L., 1999. Process Analysis. Office of Research and Development,

Washington, DC. Science Algorithms of the EPA Models-3 Community Multi-scale Air Quality (CMAQ) Modeling System, US EPA Report No. EPA/600/R-99/030 (Chapter 16).
Gu, B., et al., 2014. Agricultural ammonia emissions contribute to China's urban air pollution. Front. Ecol. Environ. 12, 265–266.
Guenther, A., et al., 2006. Estimates of global terrestrial isoprene emissions using MEGAN (model of emissions of gases and aerosols from nature). Atmos. Chem. Phys. 6 (11), 3181–3210.
Huang, R.-J., et al., 2014. High secondary aerosol contribution to particulate pollution during haze events in China. Nature 514, 218–222.
Itahashi, S., et al., 2019. MICS-asia III: Overview of Model Inter-comparison and Evaluation of Acid Deposition over Asia 53.
Itahashi, S., et al., 2017. Nitrate transboundary heavy pollution over East Asia in winter. Atmos. Chem. Phys. 17, 3823–3843.
Jo, Y.J., et al., 2020. Changes in inorganic aerosol compositions over the Yellow Sea area from impact of Chinese emissions mitigation. Atmos. Res. 104948.
Kim, B.-U., et al., 2017a. Spatially and chemically resolved source apportionment analysis: case study of high particulate matter event. Atmos. Environ. 162, 55–70.
Kim, H.C., et al., 2017b. Regional contributions to particulate matter concentration in the Seoul metropolitan area, South Korea: seasonal variation and sensitivity to meteorology and emissions inventory. Atmos. Chem. Phys. 17, 10315–10332.
Kim, E., et al., 2021. Direct and cross impacts of upwind emission controls on downwind PM2.5 under various ammonia conditions. Environ. Pollut. 268 (Part A), 115794.
Lachatre, M., et al., 2019. The unintended consequence of SO2 and NO2 regulations over China: increase of ammonia levels and impact on PM2.5 concentrations. Atmos. Chem. Phys. 19, 6701–6716.
Lee, H.J., et al., 2019. Impacts of atmospheric vertical structures on transboundary aerosol transport from China to South Korea. Sci. Rep. 9, 1–9.
Lee, H.S., et al., 1999. Seasonal variations of acidic air pollutants in Seoul, South Korea. Atmos. Environ. 33, 3143–3152.
Li, J., et al., 2007. Modeling study of ozone seasonal cycle in lower troposphere over east Asia. J. Geophys. Res. 112, D22S25.
Lin, M., et al., 2010. Quantifying pollution inflow and outflow over East Asia in spring with regional and global models. Atmos. Chem. Phys. 10, 4221–4239.
Liu, X.-H., et al., 2010. Understanding of regional air pollution over China using CMAQ, part II. Process analysis and sensitivity of ozone and particulate matter to precursor emissions. Atmos. Environ. 44, 3719–3727.
Morino, Y., et al., 2006. Partitioning of HNO_3 and particulate nitrate over Tokyo: effect of vertical mixing. J. Geophys. Res. 111, D15215.
National Institute of Environmental Research (NIER), 2016. http://airemiss.nier.go.kr/user/boardList.do?command. = view&page = 1&boardId = 74&boardSeq = 303&id = airemiss_040100000000;. (Accessed 6 October 2020).
Pinder, R.W., et al., 2008. Environmental impact of atmospheric NH_3 emissions under present and future conditions in the eastern United States: future impact OF NH_3 emissions. Geophys. Res. Lett. 35.
Pinder, R.W., et al., 2007. Ammonia emission controls as a cost-effective strategy for reducing atmospheric particulate matter in the eastern United States. Environ. Sci. Technol. 41, 380–386.
Seinfeld, J.H., Pandis, S.N., 2006. Atmospheric Chemistry and Physics: from Air Pollution to Climate Change, 3rd. John Wiley & Sons, New York, USA.
Skamarock, W.C., et al., 2008. A time-split nonhydrostatic atmospheric model for weather research and forecasting applications. J. Comput. Phys. 227 (7), 3465–3485.
Sun, W., et al., 2018. Long-term trends of anthropogenic SO_2, NO_x, CO, and NMVOCs emissions in China. Earth's Future 6, 1112–1133.
Wang, Y., et al., 2013. Sulfate-nitrate-ammonium aerosols over China: response to 2000–2015 emission changes of sulfur dioxide, nitrogen oxides, and ammonia. Atmos. Chem. Phys. 13, 2635–2652.
Woo, J.-H., et al., 2020. Development of the CREATE inventory in support of integrated climate and air quality modeling for Asia. Sustainability 12, 7930.
Zhang, J., et al., 2017. Cost-effectiveness optimization for SO 2 emissions control from coal-fired power plants on a national scale: a case study in China. J. Clean. Prod. 165, 1005–1012.
Zhang, H., et al., 2012. Source apportionment of PM2.5 nitrate and sulfate in China using a source-oriented chemical transport model. Atmos. Environ. 62, 228–242.
Zhao, M., et al., 2016. Variation of urban atmospheric ammonia pollution and its relation with PM2.5 chemical property in winter of beijing, China. Aerosol Air Qual. Res. 16, 1390–1402.
Zheng, B., et al., 2018. Trends in China's anthropogenic emissions since 2010 as the consequence of clean air actions. Atmos. Chem. Phys. 18, 14095–14111.